Journal of Biomedical Optics

BiomedicalOptics.SPIEDigitalLibrary.org

Autofluorescence imaging of basal cell carcinoma by smartphone RGB camera

Alexey Lihachev
Alexander Derjabo
Inesa Ferulova
Marta Lange
Ilze Lihacova
Janis Spigulis

SPIE.

Autofluorescence imaging of basal cell carcinoma by smartphone RGB camera

Alexey Lihachev,[a,*] Alexander Derjabo,[b] Inesa Ferulova,[a] Marta Lange,[a] Ilze Lihacova,[a] and Janis Spigulis[a]
[a]University of Latvia, Institute of Atomic Physics and Spectroscopy, Biophotonics Laboratory, Raina Boulevard 19, Riga LV-1586, Latvia
[b]Riga East University Hospital, Oncology Centre of Latvia, Hipokrata Street 4, Riga LV-1079, Latvia

Abstract. The feasibility of smartphones for *in vivo* skin autofluorescence imaging has been investigated. Filtered autofluorescence images from the same tissue area were periodically captured by a smartphone RGB camera with subsequent detection of fluorescence intensity decreasing at each image pixel for further imaging the planar distribution of those values. The proposed methodology was tested clinically with 13 basal cell carcinoma and 1 atypical nevus. Several clinical cases and potential future applications of the smartphone-based technique are discussed.
 [DOI: 10.1117/1.JBO.20.12.120502]

Keywords: autofluorescence; photobleaching; RGB imaging; smartphone.

Paper 150558LRR received Aug. 20, 2015; accepted for publication Nov. 12, 2015; published online Dec. 11, 2015.

1 Introduction

Incidences and mortality from skin cancer are still increasing.[1] Depending on the melanin concentration, skin tumors are broadly classified into two types—malignant melanomas (MM) and nonmelanoma skin cancers (NMSC). MM is the most aggressive skin cancer modality with death rate ~80% of all fatal skin cancer cases.[1] The most common NMSC are basal cell carcinoma (BCC, about 80% of new cases) and squamous cell carcinoma (SCC, about 20% of new cases) derived from the basal and squamous cells of the epidermis, respectively.[2] BCC is characterized by very slow growth tendency, low mortality rate, and high risk of recurrence, while SCC is more aggressive and associated with the risk of metastasis.[3,4]

Early detection and removal of skin cancers can significantly increase the survival time. Noninvasive methods in primary oncological diagnostics of skin tumors are still topical for dermatologists and oncologists worldwide. One of those is skin autofluorescence (AF) imaging and spectroscopy, based on differences of AF specific information (intensity, spectral shape, and lifetime) in the tumor and surrounding normal skin.[5–8]

The feasibility of AF spectroscopy for BCC diagnostics and differentiation has been studied extensively over this most recent decade. AF spectra from BCC lesions excited in UV/blue region (337 to 450 nm) were broadly characterized by decreased fluorescence intensity in comparison with surrounding healthy skin,[8] most often attributed to the shift in the levels of NADH/NAD+ (reduced form and oxidized form of nicotinamide adenine dinucleotide) and reduced elastin and collagen, affected by malignant process. In some cases, especially in late tumor growing stages, a weak red fluorescence peak of the endogenous porphyrins has been observed.[8]

Tissue AF usually shows the photobleaching effect,[9] which may be helpful in biomedical applications.[10–14] Under continuous wave (cw) excitation, skin AF intensity mainly drops during the first 15 to 20 s, followed by a slow decrease. Photobleaching kinetics can be well described by empirical double-exponential function with subsequent extraction of time constants τ_1 and τ_2 that characterize the rate of fast and slow phases of the AF decrease.[9] Our previous research has demonstrated that each skin pathology as well as healthy skin has its own specific AF intensity decrease kinetics depending on excitation, localization, melanin content, and blood perfusion. Furthermore, the analysis of AF decrease kinetics during the first 15 to 20 s of cw laser excitation seems to be most suitable for clinical implementation.[15,16]

Currently available smartphones equipped with high-resolution RGB cameras in combination with good light sensitivity and color representation mainly satisfy the required technical properties for adequate image acquisition.[17] This technology may become a useful diagnostic tool for dermatologists and oncologists thanks to wide accessibility, convenient use, and low cost.[18,19] However, the ability to switch off the "embedded" automatized settings such as exposure time, white balance, and ISO is crucial for the skin parametric imaging. Our latest studies have shown that smartphones such as Galaxy and Nexus are suitable for mapping of skin chromophores.[17]

So far use of smartphones in skin pathology diagnostics has been mainly related to dermatoscopy—specifically magnified image acquisition under white or color illumination with subsequent analysis based on ABCD rules, fractal image analysis or other algorithms established in dermatoscopy.[20–24] In this paper, we present a smartphone-compatible technique for acquisition and analysis of 405 nm light-emitting diode (LED) excited skin autofluorescence images.

2 Materials and Methods

2.1 *Experimental Setup*

For parametric mapping of skin AF intensity decrease rates, a sequence of AF images under continuous 405 nm LED (model LED Engin LZ1-00UA00-U8, spectral band half-width 30 nm) excitation for 20 s at a power density of ~20 mW/cm^2 with a frame rate 0.5 fr/s was recorded and analyzed. Four battery-powered violet LEDs were placed within a cylindrical light-shielding wall that also ensured fixed distance (60 mm) between the smartphone camera and evenly irradiated a spot (diameter 40 mm) of the examined tissue. A long pass filter (>515 nm) was placed in front of smartphone camera to prevent detection of the LED emission. The recorded RGB images were further separated to exploit R- and G-images for imaging of skin tissue AF

*Address all correspondence to: Alexey Lihachev, E-mail: aleksejs.lihacovs@gmail.com

1083-3668/2015/$25.00

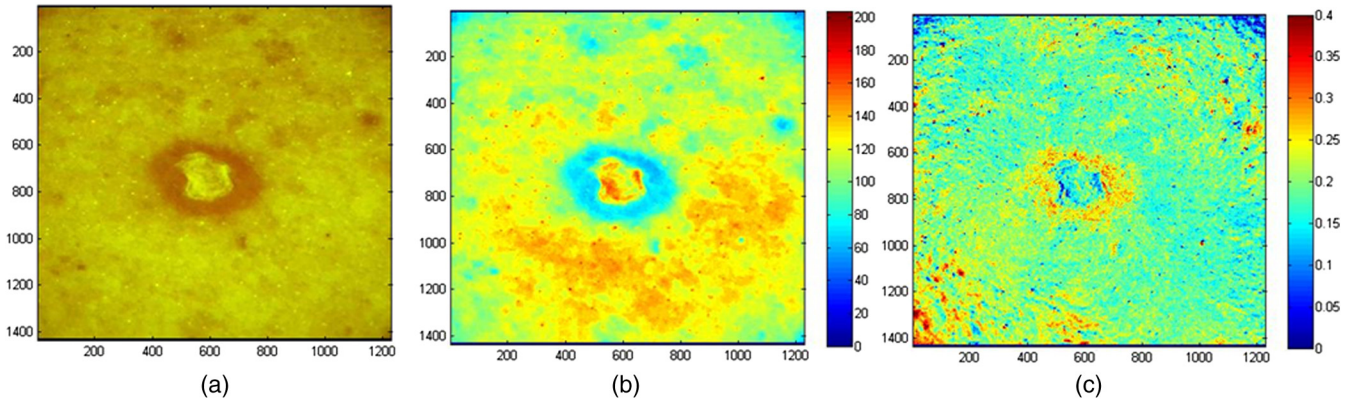

Fig. 1 Images of ulcerating basal cell carcinoma (BCC). Filtered AF color image (a) at excitation start moment, (b) the corresponding G-band image, and (c) normalized AF intensity decrease map. The pseudo color scale represents (b) the G-band intensity range and (c) the normalized AF intensity variation range.

in the red and green spectral bands, respectively. Due spectral cutoff by 515-nm long pass filter B band images in further calculations are not used. The Samsung Galaxy Note 3 smartphone comprising integrated CMOS RGB image sensor with resolution of 13 MP was used for image acquisition. All images were taken using the following settings: ISO—100, white balance—daylight, focus—manual, exposure time—fixed 200 ms.

2.2 *Image Processing*

In order to visualize the skin AF intensity decrease rates during the photobleaching, the following image processing expression was applied:

$$N(\mathrm{C}) = [I_{t0}(C) - I_t(C)]/I_{t0}(C), \quad (1)$$

where $N(C)$ represents normalized AF intensity decrease map for each pixel (or pixel group) during the excitation period, $I_{t0}[C]$—AF image at the excitation start moment, $I_t[C]$—AF image after 20 s of continuous excitation. C—color component of the RGB image—red (R), green (G), and blue (B), respectively. The values of RGB components were defined from the image data by a special program developed in MATLAB®.

Overall 50 patients with 150 different skin neoplasms (or suspicious) were inspected in the clinic. For the detailed image analysis 13 BCC and 1 atypical nevus were selected. This study was approved by the Ethics Committee of the Institute of Experimental and Clinical Medicine, University of Latvia. All involved volunteers were informed about the study and signed required consent.

3 Results and Discussion

A total of 10 solid and 3 ulcerating BCCs were selected for the study. In all BCC cases (confirmed by cytological examination) the AF images showed lowered AF intensity in malignant tissue as compared with the healthy surrounding skin, which may be attributed to decreased levels of fluorophores and increased blood perfusion caused by the malignancy process.[2,5,7] AF spectra from *in vivo* BCC under 405 nm excitation are characterized by broad (450 to 750 nm) emission spectrum with maximum in green spectral region (510 to 530 nm). In comparison with surrounding healthy skin, the intensity of AF from malignant tissue usually are lower, while the shape of the spectrum remains unchanged. Moreover, the intensity of AF is strictly correlated with the tumor pigmentation, specifically, the higher the pigmentation, the lower is the intensity of fluorescence.[2,8] In all BCC cases, the G-band (corresponding to the AF maximum) AF intensity images in comparison with R-band images showed the more pronounced intensity contrast within the tumor tissue

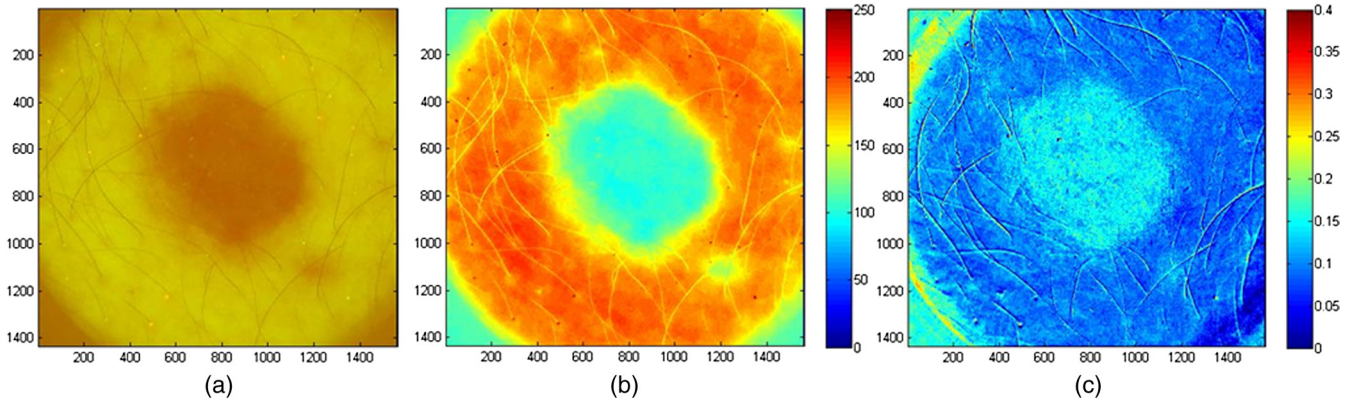

Fig. 2 Images of solid BCC. Filtered AF color image (a) at excitation start moment, (b) the corresponding G-band image, and (c) normalized AF intensity decrease map. The pseudo color scale represents (b) the G-band intensity range and (c) the normalized AF intensity variation range.

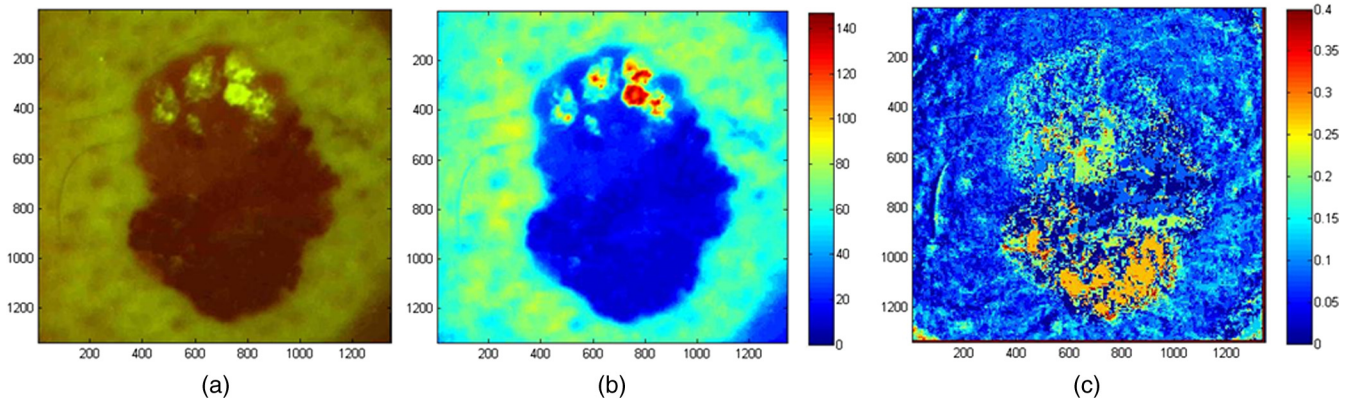

Fig. 3 Color filtered AF image of skin atypical nevus (a) at the excitation start moment, (b) the corresponding G-band image and (c) normalized AF intensity decrease map. The color scale at (b) image represents G-band intensity range and at (c) image—range of normalized AF intensity variations.

and surrounding healthy skin. Moreover, G-band AF decrease maps showed more structured compositions at tumor area in comparison with R-band AF decrease maps. In the cases of solid BCCs the AF images showed clearly bordered tumor areas with relatively low AF intensity in comparison with surrounding healthy skin. Whereas the ulcerating BCCs can be characterized by the high AF intensity in the ulcerating part surrounded by clearly bordered tissue emitting relatively low AF intensity. Furthermore, in all BCC cases the normalized AF intensity decrease maps showed high AF intensity decrease rates at the tumor areas with low AF intensity in comparison with the surrounding healthy skin and the internal ulcerating area.

Figure 1 represents images of ulcerating BCC: (a) filtered AF image at the excitation start moment, AF intensity G-band image (b), and parametric map of normalized AF intensity decrease rates in the green band (c). AF intensity image [Fig. 1(b)] shows high AF intensity in the ulcerating part (pathology center), surrounded by clearly bordered tissue emitting relatively low AF intensity. Furthermore, the AF intensity decreasing is more intensive at the external tumor area exposures in comparison with the surrounding healthy skin and the internal ulcerating area [Fig. 1(c)].

Another case of solid BCC is presented in Fig. 2. G-band AF intensity image [Fig. 2(b)] shows relatively low intensity within the tumor area with clear margins between tumor and surrounding healthy skin. The tumor area also shows higher AF intensity decrease rate [Fig. 2(c)] in comparison with the surrounding healthy skin. Besides, the images presented in Fig. 2 reveal a small area with lowered fluorescence located at "five o'clock" from the main tumor. The low AF intensity and high AF intensity decrease rate in that skin area similarly indicates to cancerous process, which is probably determined by multicentric tumor growing process.

In addition, one atypical nevus was selected for the study (Fig. 3). The nevus before surgical excision was suspected as melanoma; histological analysis of the removed tissue samples had confirmed three different types of tissue cells within the lesion area. Specifically, the upper part of the pathology mostly prevailed by intradermal nevus, the middle part by dysplastic nevus, and the lower part by junctional nevus. Normalized AF decrease distribution map [Fig. 3(c)], on the other hand, showed the fastest intensity decrease in the lower (junctional nevus) and upper side (intradermal nevus), while the middle part (dysplastic nevus) of lesion photobleached slower. The observed different AF photobleaching rates most probably are associated with different tissue fluorophore concentration, melanin content, localization, and metabolic state.

4 Conclusions

Smartphone AF imaging has shown potential for remote primary evaluation of cancerous or suspicious skin tissues. The proposed noninvasive technique and method adequately (with respect to the available literature data) represented planar distribution of AF intensities in malignant and healthy tissues. Moreover, the temporal analysis of AF intensity during the photobleaching showed a potential to be used as an additional indicator for demarcation of suspicious tissues. It may find clinical implementation, e.g., for primary evaluation of BCC, such as determination of precise excision margins prior to surgery, adequate selection of treatment method (in the case of multicentric growing process the nonsurgical methods are more desirable for the patients), as well as in selective application of immune response modulators for BCC therapy. The proposed excitation band around 405 nm covers the absorption maxima of several porphyrines and may find applications in photodynamic diagnostics of superficial nonmelanoma lesions. The most intriguing result of this research was the fact that AF photobleaching rate map showed quantitative correlation with the histology tests in the case of atypical dysplastic nevus. To explain, one can assume that specific tissue fluorophores might have individual bleaching kinetics features, which eventually could provide information on fluorophore concentration and environmental factors. The increased photobleaching rates in the tumor area most probably indicate different fluorophore content composition affected by the tumor growing process, e.g., destruction of collagen elastin cross-links along with decrease in NADH levels. Undoubtedly, this phenomenon requires additional studies to clarify the exact mechanism of uneven photobleaching of skin fluorophores under continuous optical excitation.

Acknowledgments

This work was supported by the European Regional Development Fund project "Innovative technologies for optical skin diagnostics" (No. 2014/0041/2DP/2.1.1.1.0/14/APIA/VIAA/015).

References

1. American Cancer Society, "Cancer facts & figures," (2009), http://www.cancer.org.
2. E. Drakaki et al., "Spectroscopic methods for the photodiagnosis of nonmelanoma skin cancer," *J. Biomed. Opt.* **18**(6), 061221 (2013).
3. E. N. Marieb and K. Hoehn, *Human Anatomy & Physiology*, 7th ed., Pearson International Edition, San Francisco, pp. 152–170 (2006).
4. S. D. Rigel et al., *Cancer of the Skin: Expert Consult*, 2nd ed., pp. 99–123, Elsevier Saunders, China (2011).
5. M. Panjehpour et al., "Laser-induced fluorescence spectroscopy for in vivo diagnosis of non-melanoma skin cancers," *Lasers Surg. Med.* **31**(5), 367–373 (2002).
6. N. P. Galletly et al., "Fluorescence lifetime imaging distinguishes basal cell carcinoma from surrounding uninvolved skin," *Br. J. Dermatol.* **159**(1) 152–161 (2008).
7. D. Chorvat and A. Chorvatova, "Multi-wavelength fluorescence lifetime spectroscopy: a new approach to the study of endogenous fluorescence in living cells and tissues," *Laser Phys. Lett.* **6**(3), 175–193 (2009).
8. E. G. Borisova, L. P. Angelova, and E. P. Pavlova, "Endogenous and exogenous fluorescence skin cancer diagnostics for clinical applications," *IEEE J. Quantum Electron.* **20**(2), 7100412 (2014).
9. H. Zeng et al., "The dynamics of laser-induced changes in human skin autofluorescence experimental measurements and theoretical modeling," *Photochem. Photobiol.* **68**(2), 227–236 (1998).
10. M. E. Darvin et al., "Optical methods for noninvasive determination of carotenoids in human and animal skin," *J. Biomed. Opt.* **18**(6), 061230 (2013).
11. H. Wang et al., "Improving skin Raman spectral quality by fluorescence photobleaching," *Photodiagn. Photodyn.* **9**(4), 299–302 (2012).
12. J. S. Goodwin and A. K. Kenworthy, "Photobleaching approaches to investigate diffusional mobility and trafficking of Ras in living cells," *Methods* **37**(2), 154–164 (2005).
13. G. Hennig, H. Stepp, and A. Johansson, "Photobleaching-based method to individualize irradiation time during interstitial 5-aminolevulinic acid photodynamic therapy," *Photodiagn. Photodyn. Ther.* **8**(3), 275–281 (2011).
14. C. Jayyosi et al., "Photobleaching as a tool to measure the local strain field in fibrous membranes of connective tissues," *Acta Biomater.* **10**(6), 2591–2601 (2014).
15. J. Spigulis, A. Lihachev, and R. Erts, "Imaging of laser-excited tissue autofluorescence bleaching rates," *Appl. Opt.* **48**(10), D163–D168 (2009).
16. A. Lihachev et al., "Investigation of in-vivo skin autofluorescence lifetimes under long-term cw optical excitation," *Quantum Electron.* **44**(8), 770–773 (2014).
17. I. Kuzmina et al., "Study of smartphone suitability for mapping of skin chromophores," *J. Biomed. Opt.* **20**(9), 090503 (2015).
18. Statista GmbH, "Number of smartphone users* worldwide from 2014 to 2019 (in millions)," (2015), http://www.statista.com/statistics/330695/number-of-smartphone-users-worldwide/ (26 November 2015).
19. S. A. Lamel et al., "Application of mobile teledermatology for skin cancer screening," *J. Am. Acad. Dermatol.* **67**(4), 576–581 (2012).
20. S. Kroemer et al., "Mobile teledermatology for skin tumour screening: diagnostic accuracy of clinical and dermoscopic image tele-evaluation using cellular phones," *Br. J. Dermatol.* **164**(5), 973–979 (2011).
21. J. Robert et al., "Early detection of malignant melanoma: the role of physician examination and self-examination of the skin," *CA Cancer J. Clin.* **35**, 130–151 (1985).
22. T. Maier et al., "Accuracy of a smartphone application using fractal image analysis of pigmented moles compared to clinical diagnosis and histological result," *J. Eur. Acad. Dermatol. Venereol.* **29**(4), 663–667 (2015).
23. S. Dreiseitl et al., "Computer versus human diagnosis of melanoma: evaluation of the feasibility of an automated diagnostic system in a prospective clinical trial," *Melanoma Res.* **19**(3), 180–184 (2009).
24. C. Massone et al., "Melanoma screening with cellular phones," *PLoS ONE* **2**(5), e483 (2007).